

Dipole excitations via isoscalar probes: The splitting of the pygmy dipole resonance in ^{124}Sn

E. G. Lanza,^{1,2,*} A. Vitturi,^{3,4} E. Litvinova,^{5,6} and D. Savran^{7,8}

¹*INFN Sezione di Catania, Catania, Italy*

²*Dipartimento di Fisica e Astronomia, Università di Catania, Italy*

³*Dipartimento di Fisica e Astronomia, Università di Padova, Italy*

⁴*INFN Sezione di Padova, Padova, Italy*

⁵*Department of Physics, Western Michigan University, Kalamazoo, Michigan 49008-5252, USA*

⁶*National Superconducting Cyclotron Laboratory, Michigan State University, East Lansing, Michigan 48824-1321, USA*

⁷*ExtreMe Matter Institute EMMI and Research Division, GSI Helmholtzzentrum für Schwerionenforschung GmbH, Darmstadt, Germany*

⁸*Frankfurt Institute for Advanced Studies, Frankfurt am Main, Germany*

(Received 21 October 2013; revised manuscript received 3 March 2014; published 4 April 2014)

Inelastic α -scattering excitation cross sections are calculated for electric-dipole excitations in ^{124}Sn based on the transition densities obtained from the relativistic quasiparticle time-blocking approximation (RQTBA) in the framework of a semiclassical model. The calculation provides the missing link to directly compare the results from the microscopic RQTBA calculations to recent experimental data measured via the $(\alpha, \alpha'\gamma)$ reaction, which show a structural splitting of the low-lying $E1$ strength often denoted as pygmy dipole resonance (PDR). The experimentally observed splitting is reproduced by the cross-section calculations, which allows us to draw conclusion on the structure of the PDR.

DOI: [10.1103/PhysRevC.89.041601](https://doi.org/10.1103/PhysRevC.89.041601)

PACS number(s): 24.30.Gd, 21.60.Jz, 25.70.-z, 25.55.-e

The study of nuclei with neutron excess have been pursued in the last years with focus on the properties of collective states. Special attention has been devoted to the electric-dipole strength at low excitation energy, the so-called pygmy dipole resonance (PDR), both in theory [1] as well as experimentally [2]. While the PDR represents an interesting new nuclear phenomenon itself, the connection of the (low-lying) $E1$ strength to the neutron skin of atomic nuclei [3–11] and to isovector parameters in the equation of state of nuclear matter [8,12–14] as well as its possible importance for reaction rates in astrophysical scenarios [15,16] has further increased the interest in the PDR region. Different microscopic models predict the presence of the low-lying PDR states below the well-know (isovector) electric giant dipole resonance (IVGDR); see Refs. [1,2] and references therein. Most calculations show similar results for the transition densities of the low-lying $E1$ strength, which often is used to “define” the PDR states: The neutron and proton transition densities are in phase inside the nucleus and, at the surface, only the neutron part contributes considerably. The investigation of the PDR by means of isovector (IV) as well as isoscalar (IS) probes provides information on the structure of the transition densities involved, which show a strong mixing of isospin character. While for isovector probes (i.e., photons) data exist for various nuclei obtained mainly in nuclear resonance fluorescence (NRF) and Coulomb excitation (for a recent overview see Ref. [2]), only recently data on the PDR using an isoscalar probe became available [17–21]. Applying the $(\alpha, \alpha'\gamma)$ coincidence method in combination with high-resolution γ -ray spectroscopy [22] allowed the study of the PDR for several semimagic stable nuclei in α -scattering experiments. The comparison with results from NRF revealed a surprising splitting of the PDR strength below the particle threshold into

two groups [17,19]: the lower-lying group of states is excited by both isoscalar and isovector probes while the states at higher energy are excited by photons only. A first qualitative comparison to calculations within the relativistic quasiparticle time-blocking approximation (RQTBA) as well as the quasiparticle phonon model (QPM) has shown good agreement with the experimental observation [19]: While the low-lying part of the $E1$ strength shows the described pattern of transition densities, which lead to an enhancement in the isoscalar $E1$ response, the higher-lying states are of transition character towards the GDR and, thus, are suppressed in the isoscalar channel. Meanwhile, similar IS- or IV-energy behavior of the low-lying $E1$ strength has been reported experimentally in inelastic scattering of ^{17}O off ^{208}Pb at low bombarding energies [23] as well as in other microscopic-model calculations for different nuclei; see, e.g., Refs. [9,24]. However, the comparison to the experimental data lacks on the isoscalar part, since the calculated IS $B(E1)$ strength cannot be directly compared to the measured α -scattering cross sections. The comparison thus remained on the “qualitative level.” In this manuscript we present calculation of α -scattering cross sections, based on the microscopic transition densities obtained in the RQTBA, within the framework of a semiclassical model to overcome this drawback in the comparison of experiment and calculation.

The relationship between the inelastic cross section and the reduced transition probabilities $B(E1)$ is clear for the Coulomb excitation or NRF (they are proportional) while it is not so evident in the relation between the isoscalar response and the inelastic excitation cross section due to an isoscalar probe. In this case it is better to calculate explicitly the inelastic cross section due to the nuclear interaction in order to establish its connection with the isoscalar transition probability. Recently, calculations along these lines have been performed [25–28] within a semiclassical model. Here we present the result for the system $\alpha + ^{124}\text{Sn}$ at $E_\alpha = 136$ MeV which has been experimentally studied in Refs. [19,20].

*lanza@ct.infn.it

The calculation of the inelastic cross sections are performed within a semiclassical model. The basic assumption is that the colliding nuclei move on a classical trajectory determined by the real part of the optical potential, while the internal degrees of freedom are described quantum mechanically. This model is known to hold for heavy-ion grazing collisions. In our specific case we consider the alpha-particle projectile scattered off by ^{124}Sn at $E_\alpha = 136$ MeV and analyze the excitation process of the target. Under these conditions, we can write the Hamiltonian as $H_T = H_T^0 + W(t)$ where H_T^0 is the internal Hamiltonian of the target and the external field W describes the excitation of T by the mean field of the projectile nucleus, whose matrix elements depend on time through the relative coordinate $\mathbf{R}(t)$. By solving the Schrödinger equation in the space spanned by the eigenstates of the internal Hamiltonian $|\Phi_\alpha\rangle$ one can calculate, nonperturbatively, the final population for each of the $|\Phi_\alpha\rangle$ states. Then the time-dependent state $|\Psi(t)\rangle$ of the target nucleus can be expressed as

$$|\Psi(t)\rangle = \sum_{\alpha} A_{\alpha}(t) e^{-iE_{\alpha}t} |\Phi_{\alpha}\rangle, \quad (1)$$

where the ground state is also included in the sum as the term $\alpha = 0$. The Schrödinger equation can be cast into a set of linear differential equations for the amplitudes $A_{\alpha}(t)$:

$$\dot{A}_{\alpha}(t) = -i \sum_{\alpha'} e^{i(E_{\alpha} - E_{\alpha'})t} \langle \Phi_{\alpha} | W(t) | \Phi_{\alpha'} \rangle A_{\alpha'}(t). \quad (2)$$

Their solutions are then used to construct the probability of exciting the internal state $|\Phi_{\alpha}\rangle$ as

$$P_{\alpha}(b) = |A_{\alpha}(t = +\infty)|^2 \quad (3)$$

for each impact parameter b . Finally, the total cross section is

$$\sigma_{\alpha} = 2\pi \int_0^{+\infty} P_{\alpha}(b) T(b) b db \quad (4)$$

by integrating P_{α} over the whole range of the impact parameters. The integral is modulated by the transmission coefficient $T(b)$ which takes into account processes not explicitly included in the model space and that take flux away from the elastic channel. A standard practice is to construct it by integrating the imaginary part of the optical potential associated to the studied reaction. When the imaginary part is not available from the experimental data we use the simple assumption of taking it as half of the real part.

The internal structure of the nucleus ^{124}Sn is provided by the relativistic quasiparticle time-blocking approximation developed in Refs. [29,30] and based on the covariant density functional with NL3 parametrization [31]. This approach is a self-consistent extension of the relativistic quasiparticle random-phase approximation [32] accounting for the quasiparticle-vibration coupling. The details of the calculations for ^{124}Sn are given in Ref. [20]. The RQTBA calculation scheme has been approved in various applications and justified by the full self-consistency and renormalization technique. The phonon space is truncated by the angular momentum of the phonons at $J^{\pi} = 6^+$ and by their frequencies at 15 MeV. The two-quasiparticle space is sufficiently large to provide decoupling of the translational spurious mode from the physical ones. Coupling to vibrations within the RQTBA does not affect this mode due to the

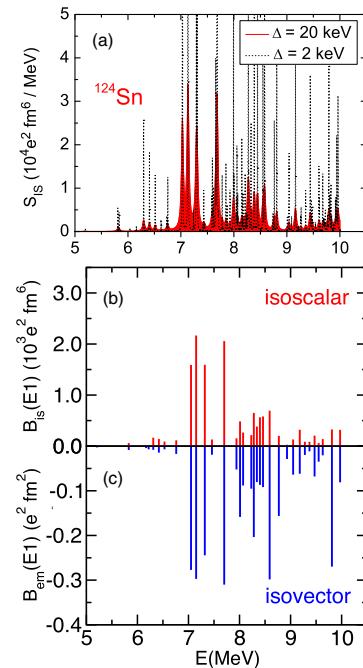


FIG. 1. (Color online) (a) Bunching procedure for the strength distribution calculated within RQTBA, and (b) the obtained isoscalar and (c) electromagnetic reduced transition probabilities of the bunched states.

subtraction of the static contribution of the particle-vibration coupling (PVC) amplitude. This subtraction also removes double counting of the PVC effects from the residual interaction, guarantees the stability of the solutions for the response function, and provides fast convergence of the renormalized PVC amplitude [33]. Here we perform a so-called bunching procedure which is illustrated in Fig. 1(a) for the isoscalar dipole strength distribution. The strength obtained with the smearing parameter $\Delta = 20$ keV is transformed into the reduced transition probabilities via the relation: $B^v = \pi \Delta S(\omega_v, \Delta)$, where $S(\omega_v, \Delta)$ is the value of the strength at the v th maximum. The bunched states obtained in this way accumulate the transition probabilities of all the states in ~ 40 keV bins. The distributions of the probabilities obtained by this procedure are displayed in Figs. 1(b) and 1(c) for the isoscalar and electromagnetic transitions, respectively. The transition densities of these bunched states are determined as described in Ref. [34] and will be used in the subsequent cross-section calculations.

The real part of the optical potential, which together with the Coulomb interaction determines the classical trajectory, is constructed with the double-folding procedure [35], as well as the nuclear form factors by double folding the RQTBA transition densities. In both cases the nucleon-nucleon interaction has been chosen to be the M3Y-Reid type [36]. Since the excitation is produced by a probe which is essentially isoscalar and with $N = Z$, only the isoscalar part of the nucleon-nucleon interaction and the isoscalar densities and transition densities contribute to the potential and to the form factors. More details are given in Ref. [28].

For the given conditions the important part of the inelastic excitation at $E_\alpha = 136$ MeV is due to the nuclear interaction.

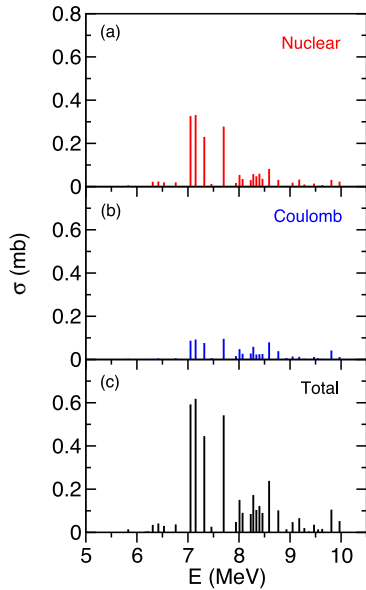


FIG. 2. (Color online) Inelastic cross sections as function of the excitation energy for the systems $\alpha + {}^{124}\text{Sn}$ at $E_\alpha = 136$ MeV. The calculations are performed when only (a) the nuclear and (b) the Coulomb interaction is switched on. (c) The results when both interactions are working.

Nevertheless, the small contribution due to the Coulomb interaction is important because of interference effects. A comparison of pure nuclear and Coulomb cross section as well as total cross section including the interference for the RQTBA bunched states is given in Fig. 2. The contribution of the Coulomb interaction [Fig. 2(b)] is small as compared with the cross section generated by the nuclear interaction [Fig. 2(a)]. When both interactions are switched on, an interference effect is produced, which results in the cross section presented in Fig. 2(c). The interference is destructive at small radii and constructive at large radii and this depends on the different structure of the nuclear and Coulomb form factor, which in turn are compelled by the fact that the isoscalar dipole transition density displays nodes. This is discussed in a more detailed way in Refs. [28,37].

The gross features of the strength distributions (see Fig. 1) are retrieved in the cross-section calculation both for the isoscalar and isovector cases. Indeed, while we know that this is mathematically true for the Coulomb case, it is not clear that the same is actually correct for the nuclear interaction. One can verify it by performing a calculation by putting the energies of the states to zero. This eliminates the contributions due to the dynamics of the reaction, such as the Q -value effect, and, at least for the Coulomb case, should produce a cross section which is proportional to the $B_{em}(EL)$ values.

Indeed, in Fig. 3(b), this is shown by plotting for each state the ratio between the Coulomb inelastic cross section and the $B_{em}(EL)$ value, calculated by putting to zero the energy of the corresponding state. As it is expected, the ratio is constant for all the states. Conversely, in the case of nuclear excitation the ratios do not have a constant value, as presented in Fig. 3(a). This corroborates the fact that, for the nuclear excitation, the individual cross section depends on the characteristics of

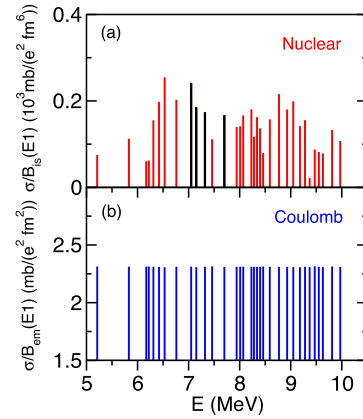


FIG. 3. (Color online) Ratios between the inelastic cross sections, calculated by putting to zero the energies of the states, to their corresponding $B(EL)$. The two panels show the results for (a) the nuclear and (b) the Coulomb excitations. The four black lines correspond to the four dipole states in Fig. 1(a) with the bigger response to the isoscalar probe.

the transition densities and one has to make calculations of the sort presented here in order to gain useful information on the excitation process.

So far the presented cross sections are implicitly integrated over the full solid angle. However, the experimental data of Refs. [19,20] were taken at the angle range from about 1.5° to 5.5° corresponding to about 1.53° to 5.94° in the c.m. system. From the deflection function shown in Fig. 4 one can deduce the ranges of impact parameters whose corresponding trajectories will end up to the experimental α -scattering-angle range. As given in Fig. 4, only the impact parameters between 8.2 to 9.0 fm and between 13.3 to 52.0 fm give contributions within the experimental angular range. Therefore, in order to be consistent with the experiment, the calculations have been repeated taking into account only the above given impact-parameter ranges. The results are shown in Fig. 5. Apart from the scale and a small variation, the general features of the three considered cross sections distributions are maintained and the decrease of the cross section for energies above 8 MeV is retrieved both for the nuclear as well as for the total cross sections.

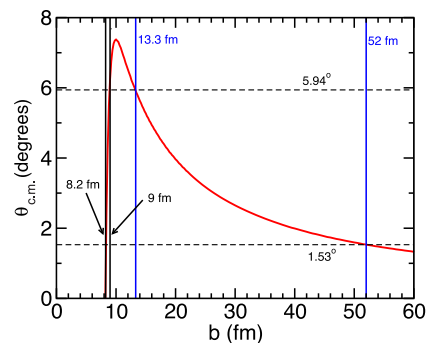


FIG. 4. (Color online) Deflection function for the system $\alpha + {}^{124}\text{Sn}$ at $E_\alpha = 136$ MeV. The horizontal dashed lines delimit the experimental α -scattering-angle range. The vertical solid line determine the corresponding impact-parameter ranges.

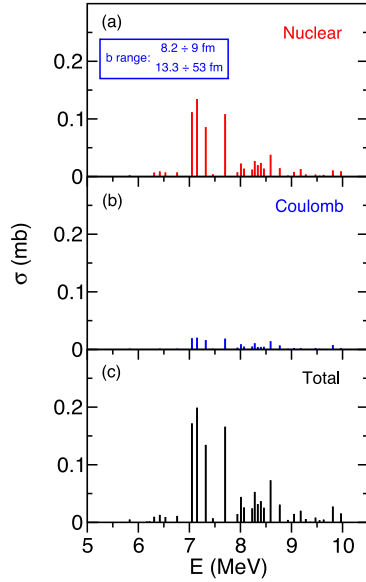


FIG. 5. (Color online) Same as Fig. 2, in this case only the impact parameters intervals whose corresponding trajectories terminate to the measured scattering-angle range are taken into account.

A comparison of the final calculated cross section based on the RQTBA and the experimental results for ^{124}Sn is presented in Fig. 6. In order to compare to the differential cross section measured in the experiment the calculations have been normalized to the corresponding solid angle. Also given are the corresponding $B_{em}(E1)$ distributions. In both cases the strongest states are about a factor of ten stronger in the RQTBA compared with experiment. This difference has the following reason: By construction, the fragmentation in the conventional RQTBA is not sufficient for a state-by-state description of the dipole strength in this energy region and coupling to higher configurations has to be included. The overall 800 keV shift of the RQTBA strength distributions has the same origin: all the strength in this energy region consists of fragments of the RQRPA pygmy mode located at about 9 MeV, and higher-order

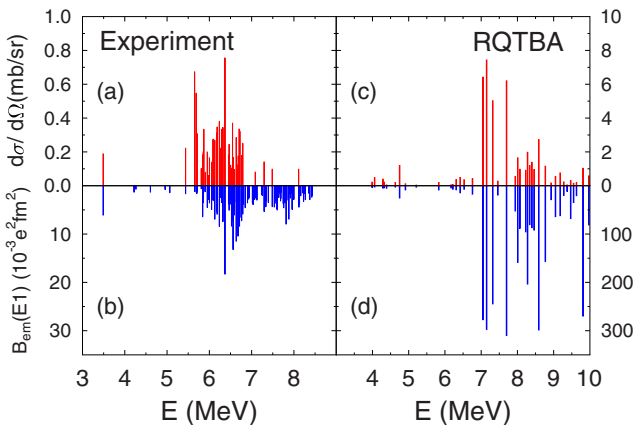


FIG. 6. (Color online) Comparison of experimental and RQTBA-based cross section for the (upper row) $(\alpha, \alpha'\gamma)$ reaction and (lower row) $B_{em}(E1)$ values for ^{124}Sn . Experimental values are taken from Refs. [20,38].

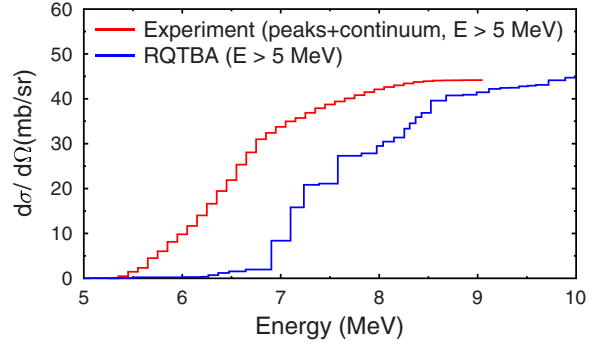


FIG. 7. (Color online) Comparison of experimental and RQTBA $(\alpha, \alpha'\gamma)$ cross sections for ^{124}Sn in terms of their cumulative sums.

correlations are expected to reinforce the fragmentation to lower energies. In addition, the bunching procedure described above results in the strength distribution of 40 keV bins rather than of the single states. However, the similar enhanced factor of about ten that we have for the cross sections and the $B_{em}(E1)$ values for the individual states show that the calculations for the cross sections are consistent and the underprediction of the fragmentation has no influence on the gross features of the two distributions. Integrating the total cross section up to 8.7 MeV results in 43.6 mb/sr for the RQTBA and 44.1 (5) mb/sr for the experiment when including also the contribution of the continuum (see Ref. [19], Fig. 3). The cumulative sums of these quantities are displayed in Fig. 7 showing that the experimental and theoretical total cross section, aside from the global energy shift, are in excellent agreement, which further supports the validity of our calculation on the absolute scale. However, one has to keep in mind that some details of the calculations may depend on the uncertainties that are connected with the use of the semiclassical model and the associated parameters as well as of the M3Y-Reid potential.

Looking at the dependence of the strength distribution on excitation energy, a good agreement of data and calculation is observed, i.e., in both cases the α -scattering cross section is strongly reduced at higher excitation energies compared to the isovector channel. This is in agreement with the qualitative comparison previously given in Ref. [19]. The proper calculation of the α -scattering excitation cross section, thus, confirms the good agreement between the experimentally observed splitting of the low-lying $E1$ strength and the results of the RQTBA calculation. However, we are aware of the fact that the NL3 interaction used in the microscopic-structure calculations produce a neutron skin which is bigger with respect to the experimental data. How this fact can affect the calculated cross section is not easy to find out and it is out of the scope of this work. Further work has to be dedicated to this delicate problem. However, our calculations show, beyond any doubt, that the same separation is found in the cross-section calculations making in this way the comparison between experiment and theory straightforward.

In summary, we have presented the calculation of α -scattering excitation cross sections for $J^\pi = 1^-$ states based on the results of microscopic calculations in the RQTBA model using a semiclassical framework for the reaction. The aim of this work is to verify that the excitation cross section due

to an isoscalar probe reproduces the structure of the theoretical isoscalar $B(E1)$, whose comparison with the experimental data was done in a previous work [19] only on a qualitative level. We have shown that the comparison between experimental and theoretical cross sections confirms the different behavior of the population of the low-lying dipole states with different probes. In the calculations nuclear-Coulomb interference is included and the resulting cross sections are sensitive to the character of the transition densities as expected. The calculations allow for a direct comparison of the RQTBA model with experimental results obtained for inelastic α scattering on an absolute scale. The good agreement with the data confirms the accurate description of the corresponding

transition densities of the low-lying $E1$ strength in the RQTBA model, which shows for the low-lying group of $E1$ excitations enhanced neutron contribution on the surface of the nucleus and an isoscalar behavior in the interior. The combination of the calculations presented and the experimental data, thus, provides a first clear identification of this signature often associated with the pygmy dipole resonance.

E.L. acknowledges support from the US-NSF Grant No. PHY-1204486 and from NSCL. D.S. acknowledges support by the Alliance Program of the Helmholtz Association (HA216/EMMI). E.G.L. and A.V. acknowledge support by the Italian PRIN (Grant No. 2009TWL3MX).

-
- [1] N. Paar, D. Vretenar, E. Khan, and G. Colò, *Rep. Prog. Phys.* **70**, 691 (2007).
- [2] D. Savran, T. Aumann, and A. Zilges, *Prog. Part. Nucl. Phys.* **70**, 210 (2013).
- [3] J. Piekarewicz, *Phys. Rev. C* **73**, 044325 (2006).
- [4] A. Klimkiewicz, N. Paar, P. Adrich, M. Fallot, K. Boretzky, T. Aumann, D. Cortina-Gil, U. D. Pramanik, T. W. Elze, H. Emling *et al.* (LAND Collaboration), *Phys. Rev. C* **76**, 051603 (2007).
- [5] N. Tsoneva and H. Lenske, *Phys. Rev. C* **77**, 024321 (2008).
- [6] N. Paar, Y. F. Niu, D. Vretenar, and J. Meng, *Phys. Rev. Lett.* **103**, 032502 (2009).
- [7] A. Carbone, G. Colò, A. Bracco, L.-G. Cao, P. F. Bortignon, F. Camera, and O. Wieland, *Phys. Rev. C* **81**, 041301 (2010).
- [8] J. Piekarewicz, *Phys. Rev. C* **83**, 034319 (2011).
- [9] D. Vretenar, Y. F. Niu, N. Paar, and J. Meng, *Phys. Rev. C* **85**, 044317 (2012).
- [10] H. Nakada, T. Inakura, and H. Sawai, *Phys. Rev. C* **87**, 034302 (2013).
- [11] A. Repko, P.-G. Reinhard, V. O. Nesterenko, and J. Kvasil, *Phys. Rev. C* **87**, 024305 (2013).
- [12] P.-G. Reinhard and W. Nazarewicz, *Phys. Rev. C* **81**, 051303 (2010).
- [13] A. Tamii, I. Poltoratska, P. von Neumann-Cosel, Y. Fujita, T. Adachi, C. A. Bertulani, J. Carter, M. Dozono, H. Fujita, K. Fujita *et al.*, *Phys. Rev. Lett.* **107**, 062502 (2011).
- [14] J. Piekarewicz, B. K. Agrawal, G. Colò, W. Nazarewicz, N. Paar, P.-G. Reinhard, X. Roca-Maza, and D. Vretenar, *Phys. Rev. C* **85**, 041302 (2012).
- [15] S. Goriely, in *Nuclear Astrophysics*, edited by M. Buballa, W. Nörenberg, J. Wambach, and A. Wirzba (GSI, Darmstadt, 1998), p. 320.
- [16] E. Litvinova, H. P. Loens, K. Langanke, G. Martinez-Pinedo, T. Rauscher, P. Ring, F.-K. Thielemann, and V. Tselyaev, *Nucl. Phys. A* **823**, 26 (2009).
- [17] D. Savran, M. Babilon, A. M. van den Berg, M. N. Harakeh, J. Hasper, A. Matic, H. J. Wörtche, and A. Zilges, *Phys. Rev. Lett.* **97**, 172502 (2006).
- [18] J. Endres, D. Savran, A. M. van den Berg, P. Dendooven, M. Fritzsche, M. N. Harakeh, J. Hasper, H. J. Wörtche, and A. Zilges, *Phys. Rev. C* **80**, 034302 (2009).
- [19] J. Endres, E. Litvinova, D. Savran, P. A. Butler, M. N. Harakeh, S. Harissopulos, R.-D. Herzberg, R. Krücken, A. Lagoyannis, N. Pietralla *et al.*, *Phys. Rev. Lett.* **105**, 212503 (2010).
- [20] J. Endres, D. Savran, P. A. Butler, M. N. Harakeh, S. Harissopulos, R.-D. Herzberg, R. Krücken, A. Lagoyannis, E. Litvinova, N. Pietralla *et al.*, *Phys. Rev. C* **85**, 064331 (2012).
- [21] V. Derya, J. Endres, M. Elvers, M. Harakeh, N. Pietralla, C. Romig, D. Savran, M. Scheck, F. Siebenhühner, V. Stoica *et al.*, *Nucl. Phys. A* **906**, 94 (2013).
- [22] D. Savran, A. M. van den Berg, M. N. Harakeh, K. Ramspeck, H. J. Wörtche, and A. Zilges, *Nucl. Instrum. Methods Phys. Res., Sect. A* **564**, 267 (2006).
- [23] A. Bracco and F. C. L. Crespi, *EPJ Web of Conferences* **38**, 03001 (2013).
- [24] X. Roca-Maza, G. Pozzi, M. Brenna, K. Mizuyama, and G. Colò, *Phys. Rev. C* **85**, 024601 (2012).
- [25] A. Vitturi, E. G. Lanza, M. Andrés, F. Catara, and D. Gambacurta, *Pramana* **75**, 73 (2010).
- [26] A. Vitturi, E. G. Lanza, M. Andrés, F. Catara, and D. Gambacurta, *J. Phys.: Conf. Ser.* **267**, 012006 (2011).
- [27] E. G. Lanza, A. Vitturi, M. V. Andrés, F. Catara, and D. Gambacurta, *Nuclear Theory*, edited by A. Georgieva and N. Minkov (Heron Press, Sofia, 2010), Vol. 29, p. 162.
- [28] E. G. Lanza, A. Vitturi, M. V. Andrés, F. Catara, and D. Gambacurta, *Phys. Rev. C* **84**, 064602 (2011).
- [29] E. Litvinova, P. Ring, and V. Tselyaev, *Phys. Rev. C* **78**, 014312 (2008).
- [30] E. Litvinova, P. Ring, V. Tselyaev, and K. Langanke, *Phys. Rev. C* **79**, 054312 (2009).
- [31] G. A. Lalazissis, J. König, and P. Ring, *Phys. Rev. C* **55**, 540 (1997).
- [32] N. Paar, P. Ring, T. Nikšić, and D. Vretenar, *Phys. Rev. C* **67**, 034312 (2003).
- [33] V. I. Tselyaev, *Phys. Rev. C* **88**, 054301 (2013).
- [34] E. Litvinova, P. Ring, and V. Tselyaev, *Phys. Rev. C* **75**, 064308 (2007).
- [35] G. R. Satchler and W. G. Love, *Phys. Rep.* **55**, 183 (1979).
- [36] G. Bertsch, J. Borysowicz, H. McManus, and W. G. Love, *Nucl. Phys. A* **284**, 399 (1977).
- [37] F. Catara, E. G. Lanza, M. A. Nagarajan, and A. Vitturi, *Nucl. Phys. A* **624**, 449 (1997).
- [38] K. Govaert, F. Bauwens, J. Bryssinck, D. De Frenne, E. Jacobs, W. Mondelaers, L. Govor, and V. Y. Ponomarev, *Phys. Rev. C* **57**, 2229 (1998).